Received: 2 December 2016 | Revised: 28 January 2018 | Accepted: 16 May 2018

DOI: 10.1002/qj.3333

RESEARCH ARTICLE

Quarterly Journal of the Royal Meteorological Society RMetS

Coupling between radiative flux divergence and turbulence near the surface

Pierre Gentine[1] | Gert-Jan Steeneveld[2] | Bert G. Heusinkveld[2] | Albert A.M. Holtslag[2]

[1]Earth and Environmental Engineering, Earth Institute, Columbia University, New York, New York,
[2]Meteorology and Air Quality Section, Wageningen University, Wageningen, The Netherlands

Correspondence
Pierre Gentine, Earth and Environmental Engineering, Earth Institute, Columbia University, 500 W 120th Street, Room 842D, Mailcode 4711, New York, NY 10027, USA.
Email: pg2328@columbia.edu

Funding information
Biological and Environmental Research, Early Career. Division of Atmospheric and Geospace Sciences, CAREER. NASA, NIP 13-0095.

Near-surface turbulent flux and radiation divergence field observations are analysed over a grass-covered surface located at the Wageningen observatory, the Netherlands. Net radiative flux divergence appears to be a large component of the energy budget near the surface, accounting for a cooling rate of several tens of degrees per day. Long-wave radiation divergence dominates this radiation divergence flux. We show here that long-wave flux divergence near the surface is strongly coupled to sensible heat flux, except in high relative humidity (>90%) and foggy conditions. The net long-wave radiative flux divergence exhibits a sharp gradient within the first 20 m above the surface. This flux divergence is itself strongly coupled to sensible heat flux through adjustments in surface-layer profiles. Nonetheless, no systematic effect of radiation is witnessed on the turbulent temperature spectrum so that the main effect of near-surface radiation is on the mean heat budget. As typical flux-gradient relationships are derived based on observations taken in the near-surface boundary-layer region where sharp long-wave divergence is present, we suspect that those relationships implicitly represent some of the long-wave divergence term. A modification of Monin–Obukhov Similarity Theory to include the effect of radiative divergence is proposed and discussed. This calls for independent measurements of turbulent fluxes and radiative flux divergence near the surface to re-derive turbulent flux-gradient relationships independently of radiative effects.

KEYWORDS
flux-gradient relationship, radiation divergence, sensible heat flux, turbulent kinetic energy, turbulent potential energy

1 | INTRODUCTION

Radiation is an essential component of the dynamics of the planetary boundary layer (PBL). Therein, radiation divergence can be either a heat source or sink (Garratt and Brost, 1981; Nieuwstadt and Businger, 1984; Dias and Brutsaert, 1998; Ha and Mahrt, 2003; Hoch *et al.,* 2007; Steeneveld *et al.,* 2010) and is especially large in regions of sharp vertical gradients of temperature and greenhouse gases (e.g. moisture), such as in the surface layer. Radiation regulates the state of stable (Steeneveld *et al.,* 2010) and cloudy boundary layers (Randall, 1980; Deardorff, 1981; Moeng *et al.,* 1999; Stevens *et al.,* 2001; Rauber *et al.,* 2007) and the transition from the nocturnal stable to daytime unstable boundary layer (Edwards *et al.,* 2014). Radiation divergence also strongly impacts on boundary-layer entrainment (Randall, 1980; Deardorff, 1981; Moeng *et al.,* 1999; Fang *et al.,* 2013a; 2013b; Edwards *et al.,* 2014). In addition, radiation can be either a source or sink of turbulent potential energy in clear-sky (Coantic and Simonin, 1984; Dias and Brutsaert, 1998; Dias, 2013) and cloudy boundary layers (Albrecht, 1991; Wang and Albrecht, 2000; Fang *et al.,* 2013a; 2013b), and can generate or destroy turbulent kinetic energy.

Substantial understanding of boundary-layer turbulence has been gained in the last decades using *in situ* observations (e.g. Baldocchi *et al.,* 2001; Gu and Baldocchi, 2002; Holtslag, 2014) and high-resolution numerical models (Deardorff, 1970; Mason, 1989; Sorbjan, 1991; Bechtold *et al.,* 1996; Khanna and Brasseur, 1997; Sullivan *et al.,* 1998; Moeng *et al.,* 1999; Stevens and Moeng, 1999; Fedorovich *et al.,*

2004; Schmidt and Schumann, 2006; Huang and Bou-Zeid, 2013). Except for the case of stratocumulus-topped PBLs, studies of the role of radiation in PBLs have seriously lagged behind those on turbulence. This is surprising since, in many cases, radiation is one of the primary drivers of the PBL state. In the stable boundary layer, for instance, radiation divergence is a major – and often the main – component of the heat budget (Sterk *et al.,* 2013; Edwards *et al.,* 2014; Kleczek *et al.,* 2014) and is therefore key to accurately predict northern latitude temperature (Pithan and Mauritsen, 2014), a major source of uncertainty in climate models (Bony *et al.,* 2006). On larger spatial scales and longer time-scales, radiation divergence, turbulence and the surface energy and water budgets are intimately coupled (Betts *et al.,* 2013). It is thus essential to correctly characterize the magnitude of radiation divergence in the PBL and its relation to boundary-layer turbulence.

One of the main reasons behind the gap between turbulence and radiation studies is due to the limited number of observational campaigns including measurements of radiative flux divergence. To our knowledge only a select set of studies have included measurements of both turbulence and radiative flux divergence, such as over Greenland (Drüe and Heinemann, 2007; Hoch *et al.,* 2007), Antarctica (Genthon *et al.,* 2013), the Netherlands (Steeneveld *et al.,* 2010), dry tropical conditions (Niger) (Estournel *et al.,* 1986), transition regimes, such as during the Boundary Layer Late Afternoon and Sunset Turbulence field campaign (Blay-Carreras *et al.,* 2014; Lothon *et al.,* 2014), and midlatitude climate (Kansas) (Burns *et al.,* 2003). Even the mere sign of radiation divergence in the surface layer is not correctly understood (Stull, 1988), pointing to our limited knowledge of the process.

In this article we investigate the role of radiation divergence and its relationship with turbulence in the surface layer, and in particular sensible heat flux, using long-term *in situ* observations collected at the Wageningen Meteorological Observatory, the Netherlands (Steeneveld *et al.,* 2010). Our primary objective is to shed light on the coupling between radiation divergence and turbulence in the lower surface layer, both in the mean (temperature) and variance (turbulent potential energy).

The article is organized as follows. In section 2, we present the data collected at the Wageningen observatory. In section 3, we investigate the coupling between radiative flux divergence and the temperature spectrum. In section 4, we investigate the coupling between radiation and temperature gradient and sensible heat flux. In section 5, we give recommendations for further studies of radiation divergence and high-frequency measurements. Conclusions are drawn in section 6.

2 | DATASET

Vertical radiative flux divergence in the surface layer occurs over short distances (first few tens of metres) corresponding to the sharp vertical variations in mean temperature and gas concentrations, requiring dense vertical profile observations in the surface layer. We use data from Wageningen University of the 'Haarweg' observatory in Wageningen, the Netherlands (51.58°N, 5.38°E, 7 m above sea level). The surface was covered with perennial ryegrass (*Lolium perenne* L.) and rough bluegrass (*Poatrivialis* L.). The grass was mown weekly during the growing season and has a typical mean height of 0.1 m and leaf area index of 2.9. The soil is classified as heavy basin clay, with a top 30 cm mixed soil to improve drainage. A schematic summarizing the different instruments and their height is provided in Figure 1.

An aspirated psychrometer placed inside a large Stevenson screen measured the air temperature, T, at 1.5 m above the surface and wet bulb temperature, Tw, at 1.4 m above the surface. Only air temperature was measured at 0.1 m above the surface using a radiation screen. Another one measured air temperature at 0.1 m above the surface. Downwelling ($S_{\downarrow}$) and upwelling ($S_{\uparrow}$) short-wave radiation were measured with pyranometers (Kipp & Zonen, Delft, Netherlands, CM11) at 1.3, 10 and 20 m. Downwelling ($L_{\downarrow}$) and upwelling ($L_{\uparrow}$) long-wave radiation were measured with a pyrgeometer (Kipp & Zonen, CG1) at 1.3 m. Those measurements were supplemented with long-wave radiometer observations (Kipp & Zonen, CG2) at 10 and 20 m, during the period 1 February to 30 June 2006. Observations were collected at 0.2 Hz and aggregated to 10 min mean values. The silicon windows of the CG2 blocks solar radiation and transmits light in the spectral range 4.5–42 μm onto two thermopile sensors, which measure both components separately. The flat window limits the field of view to 150°. The CG2 was factory calibrated outdoors against a pyrgeometer with a field of view of 180°. The CG2 has a time constant of 8 s, its nonlinearity is less than 1%. All instruments were inspected on a daily basis and cleaned if necessary (Jacobs *et al.,* 2006).

It was essential to obtain accurate assessment of biases between the different sensors. To this end, all sensors were mounted at 1.3 m for 2 months (July and August 2006) and calibrated relative to each other. At the end of the experiment the sensors were further checked for potential drifts. The sensor at 10 m was biased compared to the 1.3 m sensor by 10 W/m^2 for downwelling long-wave $L_{\downarrow}$ and by 0.3 W/m^2 for upwelling long-wave. The sensor at 20 m was biased compared to the 1.3 m sensor by 8.4 W/m^2 for downwelling long-wave $L_{\uparrow}$ and by 3.47 W/m^2 for upwelling long-wave. The measurements were corrected for the observed bias using a time-dependent linear correction. Besides uncertainties in the instruments, low visibility (usually corresponding to high humidity) atmospheric conditions could hamper meaningful radiation observations. We thus discarded rainy situations. Further description of the dataset and data quality controls is presented in Steeneveld *et al.* (2010).

Turbulent fluxes of momentum, heat and mass (H_2O and CO_2) were measured on a lattice tower instrumented with an eddy-covariance system installed at a height of 3.4 m. This system included a three-dimensional sonic anemometer (3-D

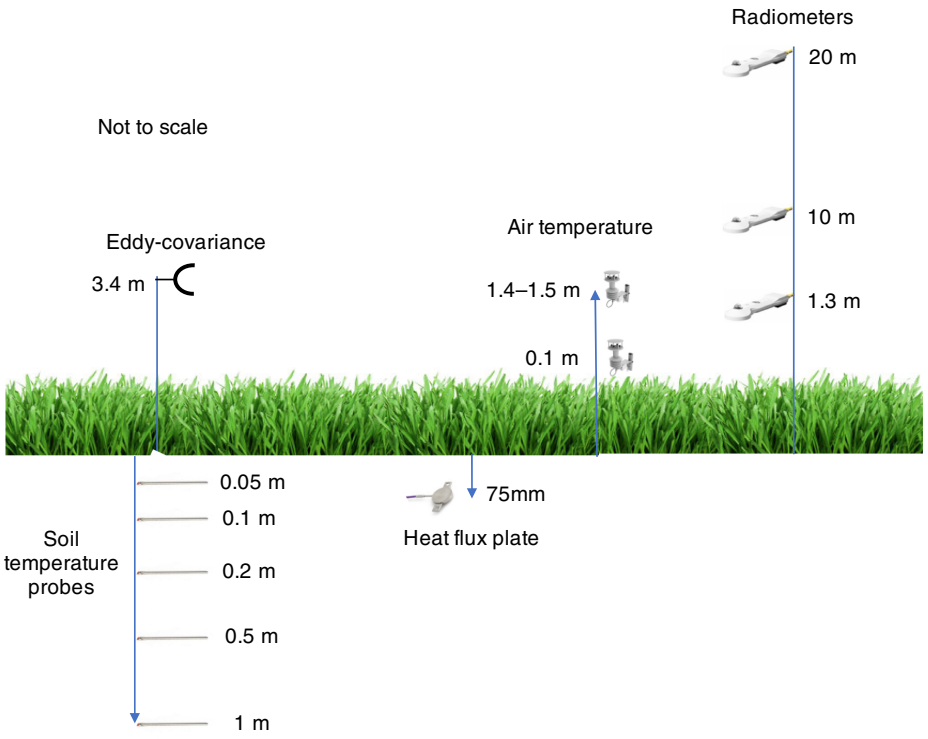

FIGURE 1 Schematics showing the position of the different instruments [Colour figure can be viewed at wileyonlinelibrary.com]

Solent, Gill Instruments Ltd., model A1012R2), and an open path infrared CO_2 and H_2O gas analyser (IRGA) (LI-COR, Inc., model LI-7500). The 3D sonic anemometer and the IRGA were set 0.05 m apart. The data were Webb-corrected for density effects due to heat and water vapour effects (Webb *et al.,* 1980).

Soil temperatures were measured with Pt-100 elements at depths 0.05, 0.10, 0.20, 0.50 and 1.0 m. The soil heat flux was measured by a heat plate (TNO, WS 31-Cp, accuracy 5%) buried at 75 mm depth. The soil heat flux at the surface was estimated using the calorimetric method correcting the ground heat flux at depth with the heat change of the layer above it (Heusinkveld *et al.,* 2004; Gentine *et al.,* 2012).

3 | RADIATION DIVERGENCE: LONG-WAVE PREDOMINANCE

3.1 | Observations

We first want to gain insights on the relative importance of the short-wave and long-wave flux divergence in the surface layer. To this end we analyse the net short-wave ΔS_{net} and long-wave ΔL_{net} radiative flux divergence between the value at 1.3 m minus the value at 20 m. The flux sign convention is taken as positive upward; a positive upward difference thus corresponds to a cooling term. In the reminder of the article, for simplicity, we use the term divergence for this difference between 1.3 and 20 m, i.e. non-normalized by the distance, except when specified.

Short-wave radiative flux divergence ΔS_{net} is relatively erratic but does exhibit a clear diurnal cycle, with higher values around noon (Figure 2), in phase with the peak in net short-wave radiation. Some erratic negative values can be observed but they cannot be due to direct solar beams, which can only reduce when passing though the atmosphere. Instead, those negative values are due to atmospheric heterogeneities from the surface, as well as turbulent anisotropy as typically observed *in situ* (Gentine *et al.,* 2011), as well as to cloudiness but also to random noise across the vertical sensors. Short-wave divergence increases sharply during sunrise and sunset (Figure 2), when the solar elevation angle is low and when radiation is more diffuse. Indeed, with diffuse light, photons are scattered in all directions and the divergence of the net short-wave in the lowest surface layer ΔS_{net} is small compared to the absolute net short-wave flux S_{net}.

Except around solar noon, in clear sky conditions, the net long-wave radiative flux divergence ΔL_{net} is the dominating flux of the radiation divergence throughout the day and is typically one or two orders of magnitude larger than the short-wave radiation divergence (Figure 2). This is not surprising; in the absence of fog, short-wave attenuation (only during daytime in the presence of solar radiation) in a layer of less than 10 m is small because the lower wavelength short-wave optical depth layer is small. In other words, in the absence of fog the near-surface atmosphere is near transparent in the short-wave but not in the long-wave. Given the preponderance of the daylong long-wave radiative flux divergence, we thus mainly focus on this term in the remainder of the article and use the term radiative flux divergence in lieu of long-wave radiative flux divergence.

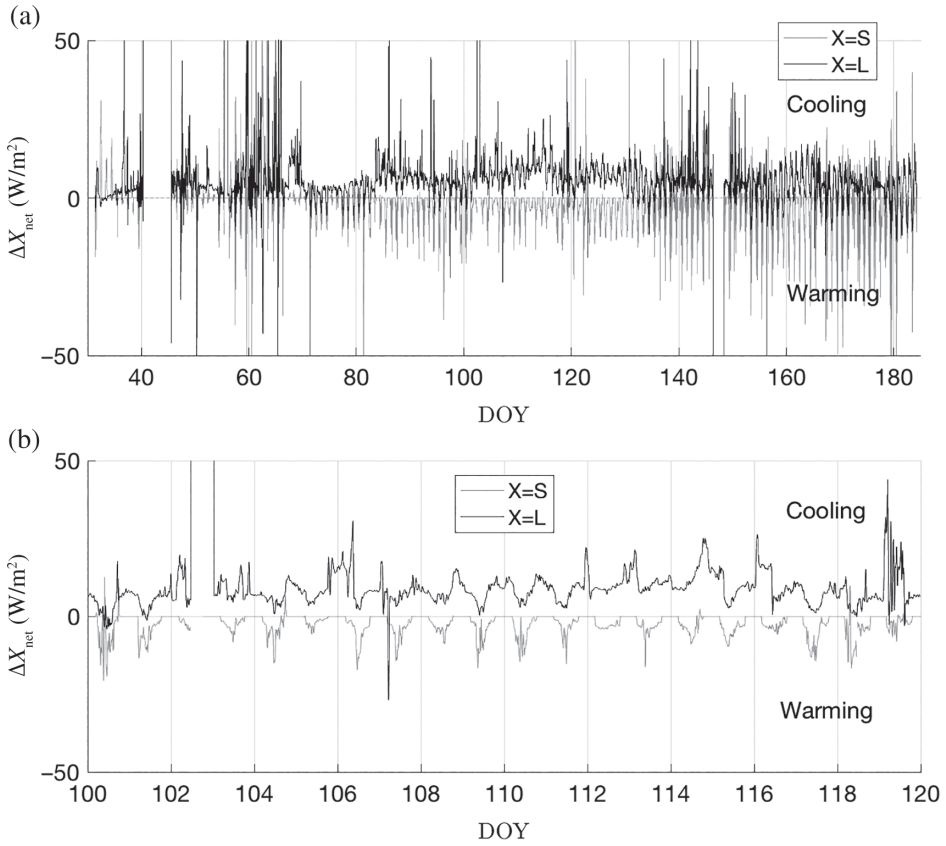

FIGURE 2 (a) Thirty-minute time series of net (downwelling minus upwelling) radiation flux of short-wave (S) or long-wave (L) at 1.3 m minus the value at 20 m, and (b) a zoom on the period between days 100 and 120

The net upward long-wave divergence ΔL_{net} between 1.3 and 20 m represents a large fraction of the net long-wave flux L_{net} near the surface (1.3 m), with a mean value ranging between 10 and 20%, depending on the meteorological conditions. This fraction exhibits substantial variability (ranging from −100 to 20% of the long-wave net flux L_{net}) throughout the course of the season. Values of $|\Delta L_{net}/L_{net}|$ larger than 50% are typical, and indicative of cloudy conditions, emphasizing the large fluctuations of ΔL_{net} with weather conditions.

Normalizing ΔL_{net} by the distance between the two measurement heights shows that most of the divergence is found below 10 m; indeed, the normalized radiation divergence ΔL_{net} between 10 and 20 m is only a relatively small fraction (less than 10%) of the total flux divergence between 1.3 and 20 m (Figure 3). The radiation divergence in the lowest part of the surface layer (<10 m) therefore dominates the total divergence. This emphasizes that most of the radiation divergence is located very close to the surface in a region where vertical gradients of temperature and water vapour are usually steep. Unfortunately, measurements below 1.3 m were not available but it is expected that the long-wave divergence will be somewhat stronger between the surface and 1.3 m. Indeed, one can estimate the difference in radiative heating between different heights, assuming a grey-body emission with constant emissivity and a near-neutral logarithmic profile of temperature. With a grass height of 0.1 m and a heat roughness length of 0.01 times the vegetation height, i.e. $z_{0h} = 0.001$ m, one finds that the flux difference ΔL_{net} between 0.1 and 1.3 m is 2.3 times stronger than between 10 and 20 m.

There are inherent challenges in measuring the long-wave divergence close to the ground, i.e. below a metre, as the observed footprint becomes very small and thus might not be representative of the larger footprint seen at higher levels. In our experiment the turbulent fluxes are evaluated at 3.4 m and net radiation is evaluated at 1.3, 10 and 20 m, while the ground heat flux is evaluated a few centimetres below the ground. The near-surface long-wave divergence could represent a substantial fraction of the surface energy and could contribute to the observed lack of surface energy balance, especially when sensors are located far away from the surface (e.g. 10 m like above tall vegetation, in order to be above the roughness sublayer).

Using a radiative transfer model with 24 levels covering the lowest 1,000 m of the atmosphere with 8 m resolution in the lowest 50 m, Cerni and Parish (1984) evaluated the mean daily radiative heating rates near the surface under horizontally homogenous conditions for climatological temperature and humidity profiles. They found heating rates of the order of −4 K/day in the Tropics, −3 K/day in midlatitude summer, −1 K/day in midlatitude winter and −2 K/day, −0.5 K/day respectively, in subarctic summer, winter respectively. Also, assuming horizontally homogeneous conditions, our observed radiative cooling near the surface is much larger than those estimates with daily values of −5 to −10 K/day in wintertime and −10 to −20 K/day in summertime (Figure 4a).

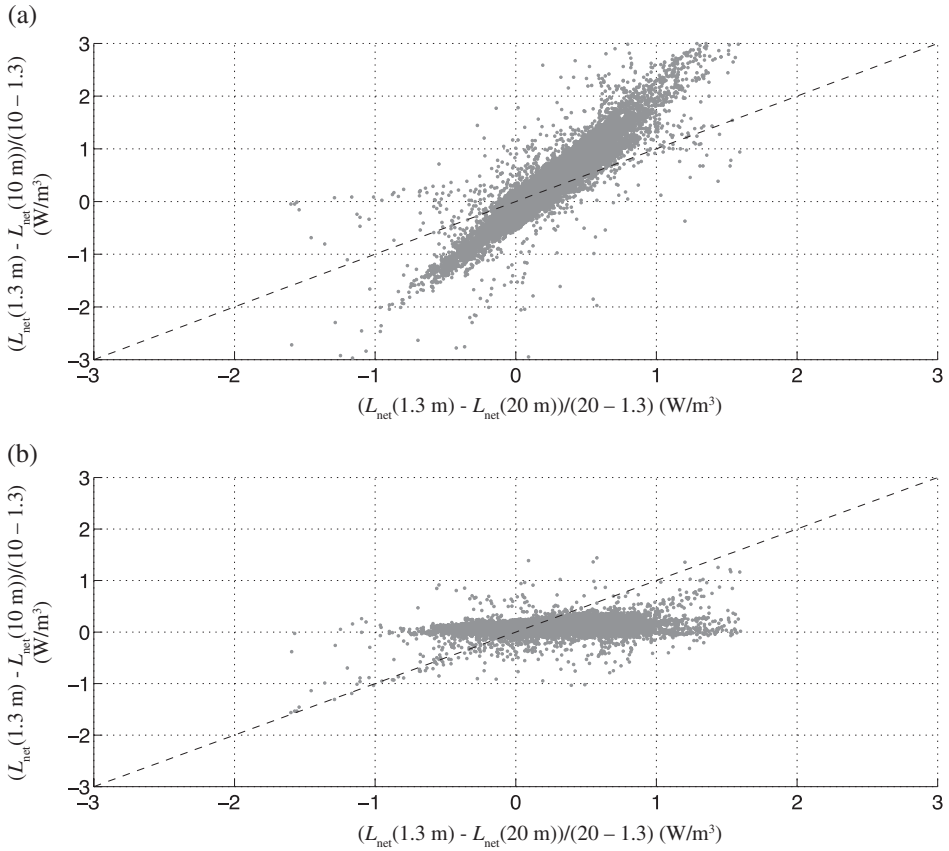

FIGURE 3 (a) Relationship between 10 min long-wave divergence computed between 1.3 and 10 m versus the value computed between 1.3 and 20 m. (b) Relationship between long-wave divergence computed between 10 and 20 m versus the value computed between 1.3 and 20 m. This result emphasizes that most long-wave divergence is located below 10 m

Sensible heat flux and specific humidity also increase during the spring and summer (Figure 4b,c) and are some of the causes of the seasonal change in the long-wave radiative heating rate, as they modify the strength of the long-wave flux gradient through changes in the air emissivity and temperature gradient (see discussion below). The measured long-wave radiative heating rate also exhibits a strong diurnal cycle, following the diurnal evolution of the vertical gradients of temperature and humidity in the surface layer, with night-time minimum values typically of the order of −20 to −50 K/day, or −0.8 to −2.1 K/h. The long-wave radiation divergence contribution to the near-surface layer energy budget is thus large.

The contribution of this long-wave component to the total PBL heat budget is clearly important, especially in shallower stable boundary layers. In the daytime convective boundary layer, the long-wave radiation contribution integrated over the entire PBL depth is smaller than the overall sensible heat flux contribution and explains why long-wave radiation is typically neglected in bulk convective boundary-layer heat budgets (Tennekes, 1973; Deardorff, 1979; Tennekes and Driedonks, 1981; Fedorovich, 1995; Gentine and Bellon, 2014). For comparison, the warming rate of potential temperature due to a typical summertime surface sensible heat flux of 100 W/m^2 is 0.3 K/h over a PBL height of 1,000 m, neglecting entrainment (entrainment has a negligible effect on the potential temperature budget of the boundary layer as it is compensated by the PBL growth (Gentine *et al.,* 2013)). In other words the sensible heat flux difference between the bottom and top of the boundary layer is of the order of 100 W/m^2. In the surface layer, radiation flux difference on the other hand typically accounts for less than 10 W/m^2, with peak values 20 W/m^2 and thus is an order of magnitude smaller than the sensible heat flux difference. When integrated over the entire PBL the radiative cooling can be much stronger, especially in the presence of stratocumulus clouds and can reach values as low as −0.25 K/h (Naumann *et al.,* 2017).

Noticeably, the atmospheric long-wave radiation divergence flux is not represented in current generation of land-surface models, as the air is assumed transparent between the surface and the height of connection with the atmospheric model or prescribed weather station height in uncoupled land-surface models, typically located between 2 and 20 m. In other words, in land-surface models the air is assumed to be transparent to radiation (e.g. Lawrence *et al.,* 2011). The transparency of the air is clearly not a valid assumption, especially in the long-wave (Figure 2). In addition, this atmospheric radiative divergence should impact their representation of the energy partitioning.

Figure 5 emphasizes the relationship between long-wave divergence, taken between 1.3 and 20 m, and surface energy balance closure ($R_n - G - H - \lambda E$). R_n is the net radiation

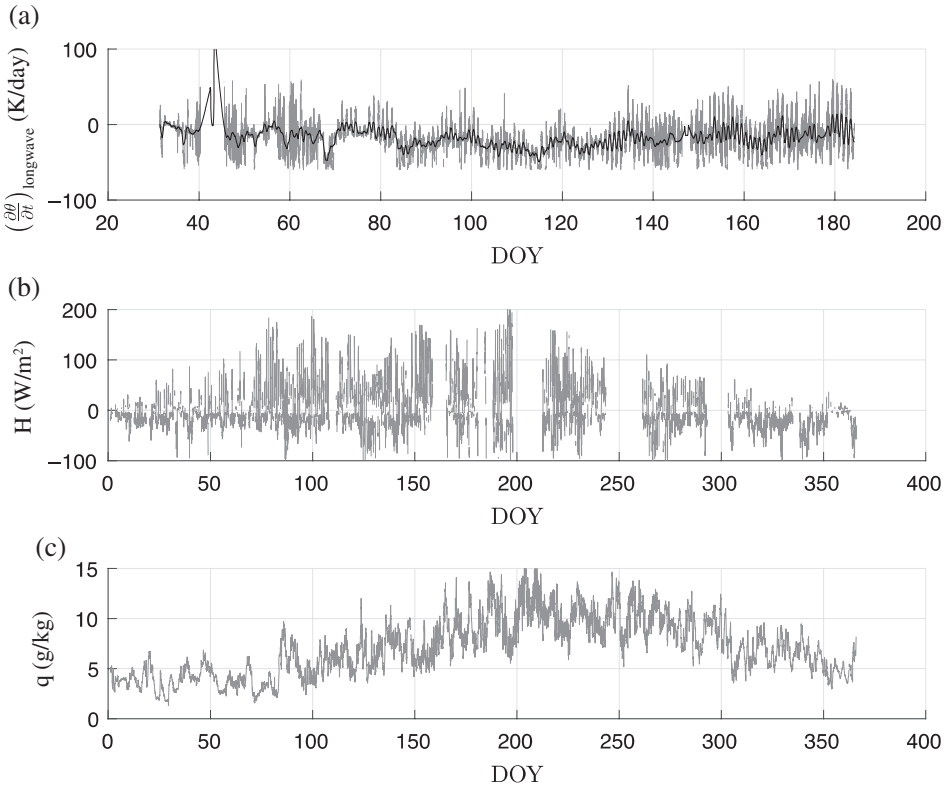

FIGURE 4 (a) Ten-minute time series of observed long-wave radiative heating between 1.3 m and 20 m, (b) 30 min time series of sensible heat flux, and (c) specific humidity. Black line in (a) represents a 3-hourly moving average of long-wave radiative heating

evaluated at 1.3 m, H and λE the sensible and latent heat flux respectively all evaluated at 3.4 m and G the surface ground heat flux. We emphasize that the net long-wave divergence computed between 1.3 and 10 m is a conservative estimate of the divergence between the surface and 1.3 m, where net radiation R_n is measured, since the long-wave divergence between the surface and 1.3 m is expected to be larger than above, as the scalar gradients are larger near the surface. In clear sky conditions, there is a positive correlation between the surface energy budget imbalance, $R_n - G - H - \lambda E$, and $-\Delta L_{net}$ (radiative heating) (Figure 5a), which suggests that long-wave radiation may explain the surface energy imbalance. In foggy situations, defined as periods with relative humidity greater than 95%, the surface energy budget imbalance is mostly uncorrelated with net long-wave divergence and also with net short-wave radiation ($R^2 = 0.003$, not shown). Radiative heating, $-\Delta L_{net}$, is more closely related to the surface budget imbalance during daytime hours ($R^2 = 0.14$), compared to night-time ($R^2 \sim 0.0$), which is nearly uncorrelated with radiative divergence, Figure 5. Indeed, at night, weak turbulence generally leads to important surface energy budget closure errors (Wilson *et al.,* 2002), as small-scale and sporadic turbulence is not entirely observed by eddy-covariance systems (Fisher *et al.,* 2007), and also because the initial subrange spectra and cospectra, of water vapour in particular, are incorrectly estimated (Mamadou *et al.,* 2016).

The lack of surface energy budget closure could also be due to vegetation heat storage. To test whether this effect could dominate the radiative divergence term

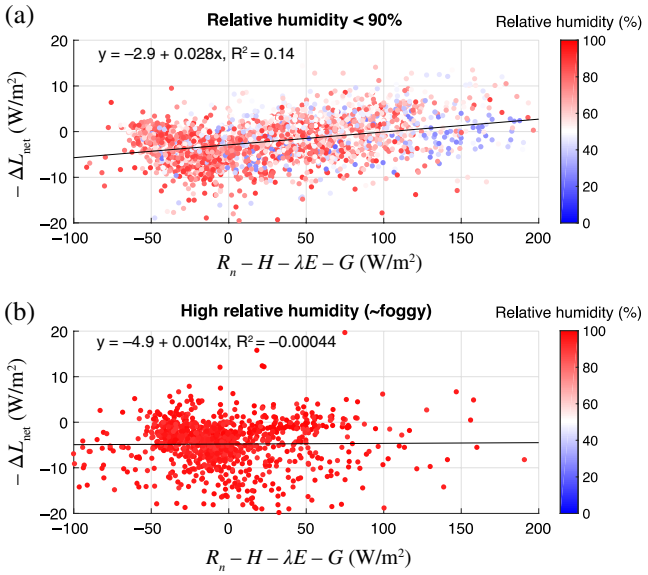

FIGURE 5 Relationship between long-wave radiative heating $-\Delta L_{net}$ between 1.3 and 10 m and surface balance imbalance, (a) in non-foggy, and (b) foggy conditions. The data is binned by relative humidity of the atmosphere (blue to red colour bar) [Colour figure can be viewed at wileyonlinelibrary.com]

we evaluated the relationship between the temporal derivative of near-surface (10 cm high) air temperature, Supporting Information Figure S1, across four different seasons: winter (December–January–February), spring (March–April–May), summer (June–July–August) and autumn (September–October–November). We did not find

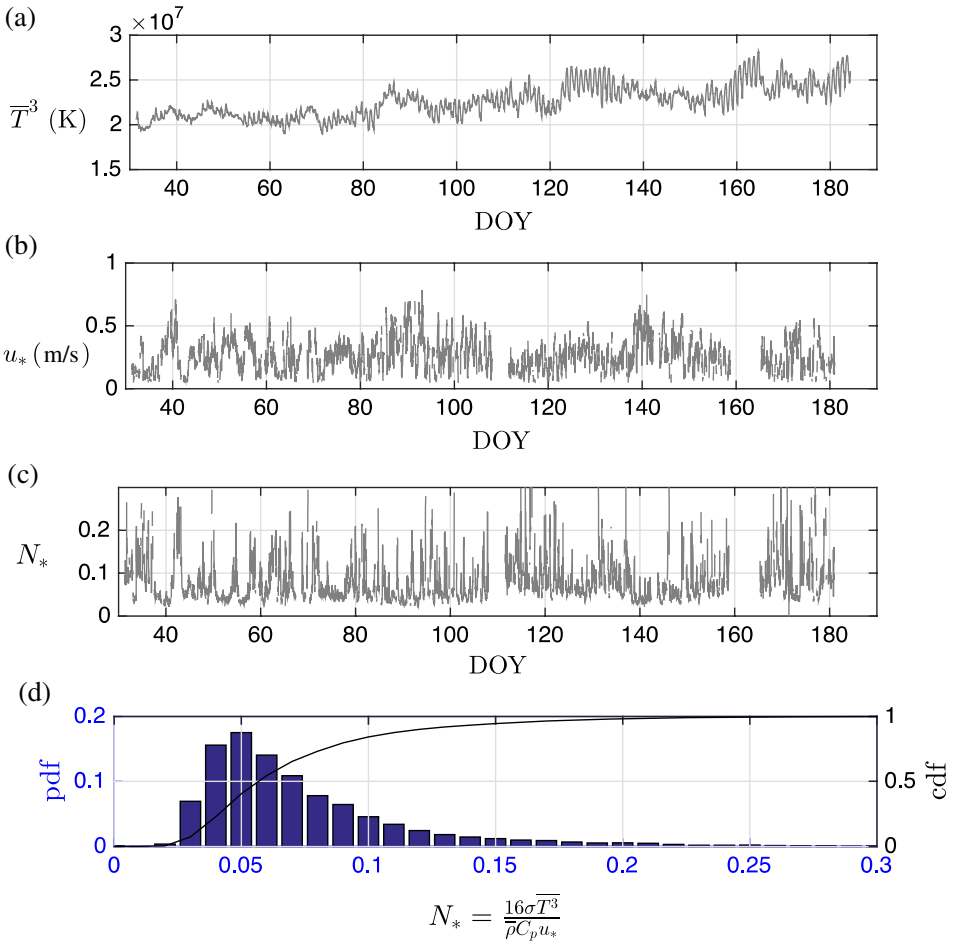

FIGURE 6 Time series (a) third moment of air temperature, (b) friction velocity, (c) N^* a dimensionless number assessing the relative importance of radiative versus turbulent dissipation of turbulent potential energy (TPE), and (d) the probability distribution function (pdf) of N^* based on 0.01 bins – blue histogram, and its cumulative distribution function – black line [Colour figure can be viewed at wileyonlinelibrary.com]

any correlation between storage and the lack of surface energy budget closure, across the four different seasons: Supporting Information Figure S2 ($R^2 < 0.06$ across seasons). This further suggests that radiative divergence is a stronger contributor to the lack of surface energy budget closure than heat storage, at least at our grass site.

Based on the previous analyses it is clear that the impact of the long-wave flux on the heat budget could be important. However, radiation not only affects the energy (temperature) budget but may also act on the turbulent potential energy (TPE) and especially on its spectrum, as it may affect the dissipation rate of TPE (Townsend, 1958; Brutsaert, 1972; Andre *et al.,* 1978; Dias and Brutsaert, 1998), which in turn feeds into the turbulent kinetic energy (TKE) (Mauritsen *et al.,* 2007). To investigate this issue, we now turn to the temperature variance budget.

3.2 | Turbulent potential energy

The potential temperature variance budget under horizontal homogeneity and with negligible advection is:

$$\frac{\partial \overline{\theta'^2}}{\partial t} = -\overline{2w'\theta'}\frac{\partial \overline{\theta}}{\partial z} - \frac{\partial \overline{w'\theta'^2}}{\partial z} - \epsilon_{\theta,\theta} - \epsilon_R, \qquad (1)$$

where the overbar denotes Reynolds' average, primes denote the turbulent anomalies, $\overline{w'\theta'}$ the turbulent vertical flux of potential temperature θ, $\overline{w'\theta'^2}$ the turbulent vertical flux of θ'^2, $\in_{\theta,\theta}$ the molecular dissipation and ϵ_R the radiative dissipation of $\overline{\theta'^2}$. The radiative dissipation terms is often represented as a fraction of the potential temperature variance, assuming local radiative dissipation closure: $\epsilon_R = \beta\overline{\theta'^2}$ (Townsend, 1958; Brutsaert, 1972; Andre *et al.,* 1978; Dias and Brutsaert, 1998).

In Fourier space, assuming homogenous and isotropic turbulence and planar homogeneity, Equation (1) becomes:

$$\frac{\partial E_{\theta,\theta}}{\partial t} = -2E_{w,\theta} - T_{\theta,\theta}\frac{\partial \overline{\theta}}{\partial z} - v_\theta k^2 E_{\theta,\theta} - E_R, \qquad (2)$$

with $E_{\theta,\theta}$ the temperature variance spectrum, $E_{w,\theta}$ the vertical velocity and temperature variance cross-spectrum, $T_{\theta,\theta}$ the temperature variance transfer term, v_θ the thermal molecular diffusion rate, k the wave number and E_R the radiative dissipation rate. A typical closure for the dissipation rate is $E_R = N(k)E_{\theta,\theta}$ (Brutsaert, 1972; Andre *et al.,* 1978; Coantic and Simonin, 1984; Dias and Brutsaert, 1998) with $N(k)$ the spectral radiative dissipation function.

In the non-foggy surface layer, the ratio of the radiative dissipation to the molecular one ($\epsilon_R/\epsilon_{\theta,\theta}$) can be assessed using

a dimensionless parameter, $N_* = 16\sigma\overline{T}^3/(\rho_0 C_P u_*)$ (Dias and Brutsaert, 1998). σ is Stefan–Boltzmann's constant, C_P the dry air specific heat and u_* the surface friction velocity. In our observations N_* ranges from 0 to 0.3, with most of the values centred around 0.05, and 98% of the values being below 0.2 (Figure 6) including foggy conditions. The $\overline{T}^3$ changes (Figure 6) only account for up to 25% of the variability of N_* and most of the N_* variability is related to variations in the friction velocity. Values of N_* larger than 0.2 correspond to regimes under which the effect of radiative dissipation on the TPE spectrum could be important (Brutsaert, 1972; Andre *et al.,* 1978; Coantic and Simonin, 1984; Dias and Brutsaert, 1998). Those higher N_* values are rare (2% of the time) and only observed in conditions of very weak surface wind, and friction velocity, as highlighted by the cumulative distribution function (Figure 6). It is indeed expected that radiative dissipation could be preponderant in still-air conditions, when turbulence is weak. These results corroborate previous theoretical analysis (Coantic and Simonin, 1984; Dias and Brutsaert, 1998 ; Dias, 2013), which emphasized that N_* should be small on Earth and correspondingly that the effect of radiative dissipation should be rarely observable on Earth, yet could be higher on other planets. If we had access to higher-resolution measurements we could define a more accurate measure of the relative efficiency of radiative to molecular dissipation but unfortunately the recorded radiation data was only available at 10 min resolution.

Under homogenous, near-steady conditions, N_* could potentially be described by Monin–Obukhov Similarity Theory (MOST) scaling. We thus evaluate the relationship between N_* and the stability parameter z/L, with L the Obukhov length (Figure 7a). As expected with the dependence of N_* on u_*, there is a strong correlation between N_* and the stability z/L, even if some spread is observed. Lowest values are observed in neutral conditions ($z/L \sim 0$), as would be expected, with N_* values scattered around 0.03.

N_* evaluates the relative efficiency of radiative dissipation compared to the molecular one on the temperature variance budget but radiation also affects the temperature budget. We therefore define a radiative length-scale $L_{\mathrm{red}} = \overline{\rho} C_p \overline{w'\theta'}/(-\partial L_{\mathrm{net}}/\partial z)$ to evaluate the distance of influence of radiative heating/cooling compared to that of sensible heat flux. Figure 7 shows the 2D histogram of z/L_{red} and N_*, as a way to relate the impact of the radiation divergence on the mean temperature budget and on the temperature variance. As the radiative flux divergence drives both processes, some correlation could be expected. Opposite to this expectation, the magnitude of the normalized flux divergence z/L_{red} and relative radiative dissipation N_* are almost uncorrelated (Figure 7b), emphasizing that radiation acts nearly independently on the temperature mean and variance. In addition, the stability z/L is relatively uncorrelated with z/L_{rad} (Figure 7c).

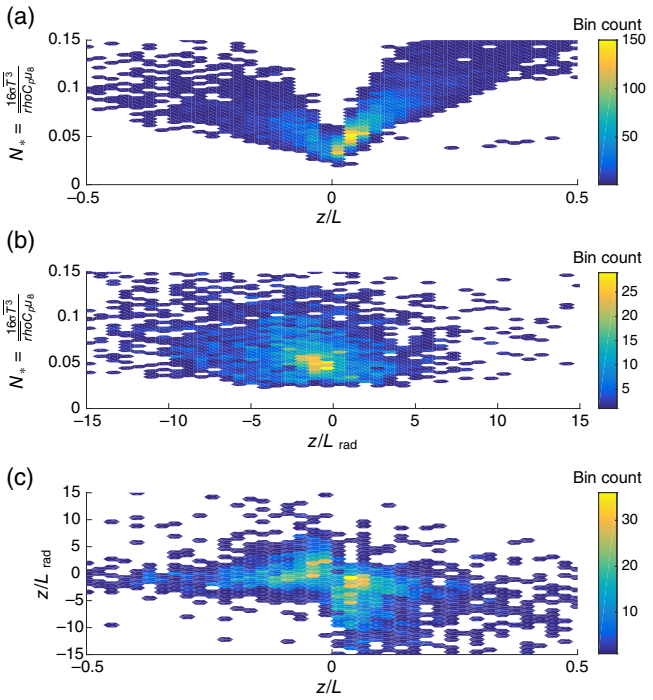

FIGURE 7 (a) 2D density plot of N^* and stability z/L, (b) density plot of N^* and z/L_{rad}, and (c) density plot of z/L_{rad} and z/L [Colour figure can be viewed at wileyonlinelibrary.com]

This emphasizes that the relative rate of radiative heating is not directly linked to the stability of the atmosphere, and other factors are influencing the radiative heating rate, as we elaborate below.

Radiative dissipation can be related to thermal molecular dissipation rate as $E_R(k) = N(k)E_{\theta,\theta}(k)$ (Dias and Brutsaert, 1998; Dias, 2013). Radiation dissipation acts on smaller wave numbers (larger eddies) because of the non-local nature of radiative transport. Schertzer and Simonin (1981) observed an inertial–radiative range characterized by a slope steeper than −3 but pointed out that this behaviour might be unlikely on Earth. Dias and Brutsaert (1998) emphasized three regimes of radiation-induced spectrum: (a) at very small k, where the continuum absorption is dominant, $N(k) \sim k^2$, (b) over a wide intermediate range of k values, in the so-called strong-line region, $N(k) \sim k$ and (c) at high wave numbers k in the weak-line region, $N(k) \rightarrow N_\infty = N_* \overline{\rho}_{\mathrm{v}} \beta_{\mathrm{p}}$ with β_{p} the Planck coefficient and $\overline{\rho}_{\mathrm{v}}$ the mean water vapour density.

A spectral analysis is performed on the turbulent time series of temperature over 30 min periods using a linear de-trending of the data (Figure 8). In our observations at Wageningen, high (>0.2) N_* values are mostly observed at very high and very low z/L. For those stabilities, the range of observed slopes of the temperature variance S_{TT} spectrum in the inertial subrange is close to −5/3, given by the Corrsin–Obukhov scaling for scalar variance in homogenous, isotropic turbulence (Kolmogorov, 1941; 1961; Kaimal *et al.,* 1976) for all N_* conditions (Figure 8). Binning turbulence spectra between low N_* (<0.025) and high N_* (>0.2) does not demonstrate any change in the temperature variance spectrum S_{TT} slope

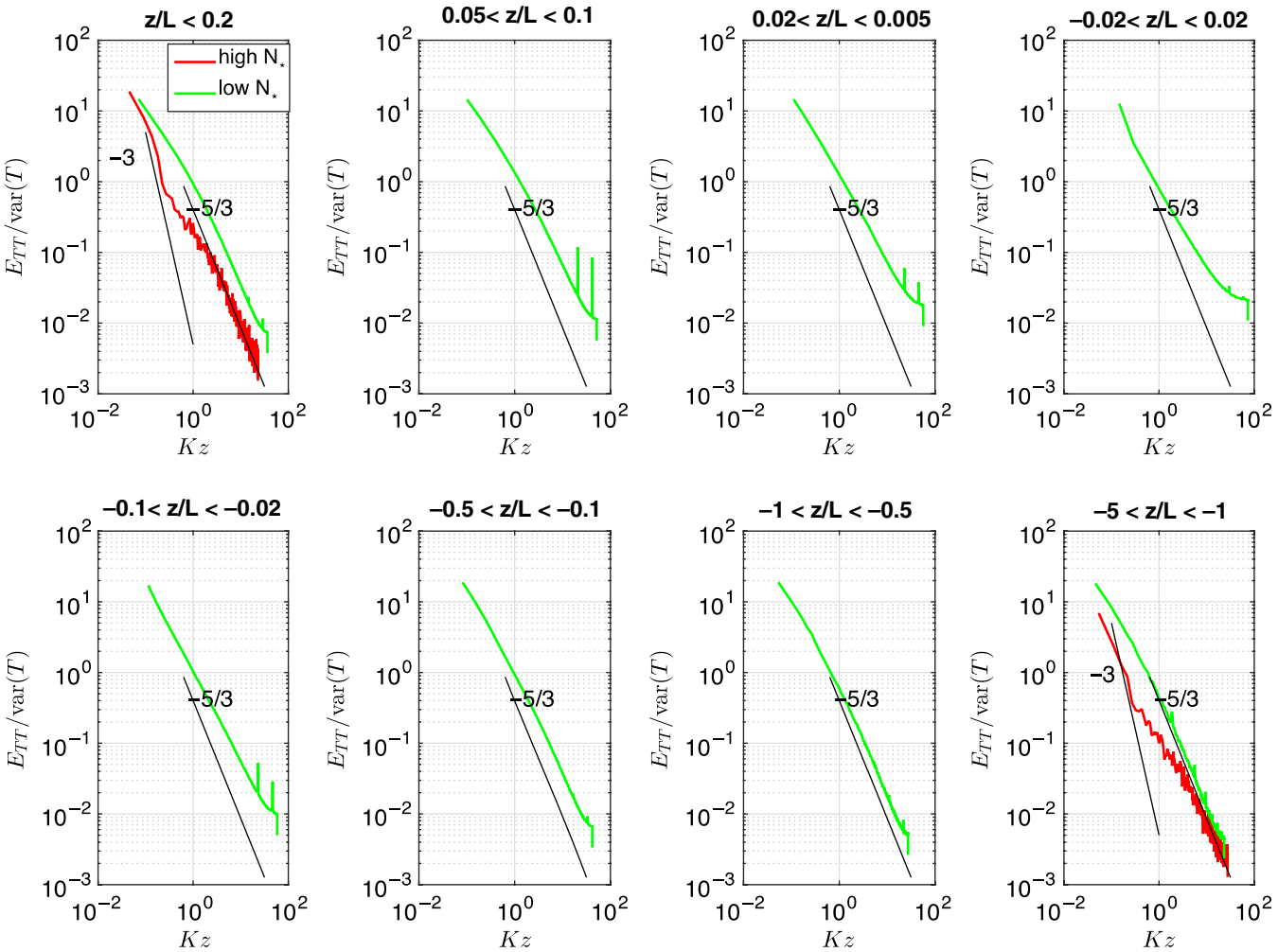

FIGURE 8 Average normalized temperature power spectra binned across varying stability conditions and N^* values. Low N^* (<0.2) values are depicted in green and high N^* (>0.2) are plotted in red [Colour figure can be viewed at wileyonlinelibrary.com]

(Figure 8), which would have been indicative of changes in the decay rate though radiation dissipation (Dias and Brutsaert, 1998). In the entire dataset there are no slopes smaller than −3, the minimum reported value of radiative-driven inertial subrange (not shown). This further indicates that the radiative effect on the inertial subrange is small, as expected in previous theoretical studies (Brutsaert, 1972; Andre *et al.,* 1978; Coantic and Simonin, 1984; Dias and Brutsaert, 1998; Dias, 2013).

In conclusion, the temperature variation spectrum seems unaffected by radiative dissipation. It is likely that the typical values of N_* observed at our site are simply too small to observe a radiative inertia subrange, which has been observed in neutral conditions with $N_* > 4.4$ for midlatitudes (Dias and Brutsaert, 1998). Possibly N_* may not be the most appropriate scaling variable for radiative dissipation compared to the molecular one. Indeed the $\overline{T}^3$ factor in N_* may not be the best scaling of the influence of the radiative divergence effect, as radiation might also relate to the curvature of the temperature profile and to trace gases (Steeneveld *et al.,* 2010). We nonetheless tried other scaling (such as ones including curvature – not shown), and we could not find regimes in which radiative dissipation would dominate molecular ones. Observation of radiation data at higher temporal resolution, in regions with high temperature and humidity (e.g. tropical) – in which we expect radiation effects to be more important – could help observe regimes in which the effects of radiative dissipation might be more important on the temperature spectrum.

4 | COUPLING BETWEEN TURBULENCE AND RADIATION DIVERGENCE

4.1 | Monin–Obukhov similarity theory and radiation

In a near-steady state, horizontally homogeneous surface layer, Monin–Obukhov Similarity Theory defines the dimensionless relationship between the temperature vertical gradient and stability. Using the Buckingham Pi theorem, neglecting the effect of moisture on buoyancy, the flow is characterized by $m = 4$ variables: potential temperature gradient $d\overline{\theta}/dz$, buoyancy flux $B = (g/\overline{\theta})\overline{w'\theta'}$, friction velocity u_* and vertical height z for $n = 3$ dimensions: time, temperature

and length. There are thus $m-n=1$ independent dimensionless quantities, functionally related. The Buckingham Pi theorem then predicts that the dimensionless potential temperature gradient is a function of a single $(m-n=1)$ non-dimensionless variable, z/L:

$$-\frac{Kzu_*}{\overline{w'\theta'}}\frac{\partial\overline{\theta}}{\partial z}=\phi_h\left(\frac{z}{L}\right), \tag{3}$$

with $L = -u_*^3\overline{\theta}/(kg\overline{w'\theta'})$, g gravity and K von Karman's constant (a value of 0.4 is used here (Högström, 1996)).

MOST does not include the effect of radiation divergence. It also implicitly assumes that the surface layer is a constant flux layer so that the scaling is applicable over the entire surface layer. Local scaling variations have been proposed as important, especially in the stable boundary layer (Holtslag and Nieuwstadt, 1986; Mahrt, 1999).

Based on the results of our previous section, we assume that radiative dissipation is negligible compared to TKE and thermal molecular dissipation and we only consider the effect of long-wave radiation divergence on the mean potential temperature budget. In the presence of long-wave divergence, neglecting short-wave divergence effects (section 3), we now have $m=5$ parameters: potential temperature gradient $d\overline{\theta}/dz$, buoyancy flux B, friction velocity u_*, vertical height z and heating tendency due to upward long-wave radiation divergence in the surface layer $\Delta L_{\mathrm{net}}/(\overline{\rho}C_p)$. The number of dimensions n has not changed when applying the Buckingham Pi theory. This means that the flow should be characterized by two (dimensionless) variables: z/L and another variable related to radiation. We use z/L_{rad} as our second variable. The temperature gradient may then be expressed as:

$$-\frac{Kzu_*}{\overline{w'\theta'}}\frac{\partial\overline{\theta}}{\partial z}=\phi_h\left(\frac{z}{L},\frac{z}{L_{\mathrm{rad}}}\right). \tag{4}$$

We note that given the vertical variability of the radiation heating rate, L_{rad} should be locally defined. This extension assumes that L and L_{rad} are independent. To test whether this assumption was reasonable, we evaluated the coupling between the two length-scales, L and L_{rad}, using for L_{rad} the value computed between 1.3 and 10 m, and assuming a vertically uniform sensible flux. Even though radiation divergence between 1.3 and 10 m differs from the one computed at the eddy covariance height (3.4 m) this is providing a reasonable first-order estimate of L_{rad}. There is some relative decoupling between the two length-scales (Figure 7c) so that the new length-scale L_{rad} is deemed appropriate. Given that we only have access to three vertical temperature levels, it is difficult to accurately evaluate the temperature gradient in Equation (4), and future work should try using many more vertical levels.

We nonetheless try to evaluate the role of the radiative cooling term on the integrated temperature gradient by determining its impact on the normalized temperature gradient, $K\frac{T_{0.1\mathrm{m}}-T_{1.5\mathrm{m}}}{T_*}$ computed between 0.1 and 1.5 m, stratified by z/L values (Figure 9). We note that the sensor temperatures were unbiased in neutral conditions. In the absence of strong radiative cooling/heating ($z/L_{\mathrm{rad}}\sim 0$), the normalized temperature gradient follows the expected heat stability correction, increasing with stability z/L. The data exhibits relatively reduced scatter. Changes in z/L_{rad} however strongly affect the normalized temperature gradient, especially in near-neutral conditions. As hypothesized, radiative cooling typically decreases the temperature gradient, and warming increases the temperature gradients. Large z/L_{rad} values (in absolute terms) generate large departure from MOST scaling of the temperature gradient. These results indicate that the radiative divergence in the surface layer affects the temperature gradient scaling and point to potential failure of MOST, or at least to incomplete characterization by MOST.

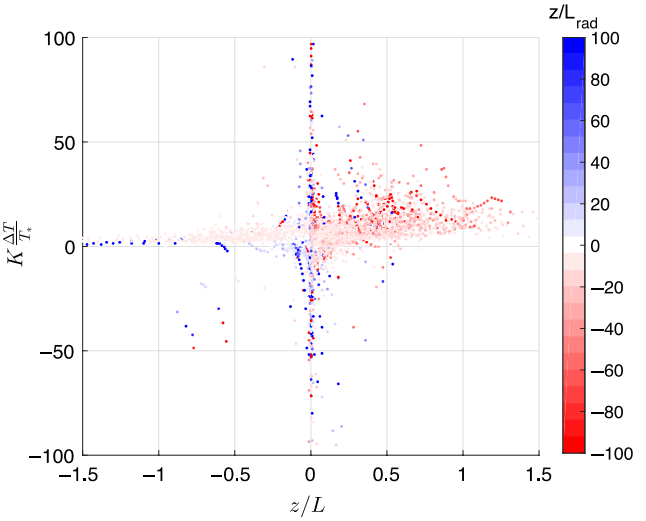

FIGURE 9 Normalized air temperature gradient as a function of stability, z/L; markers are coloured by the magnitude of z/L_{rad}. Regimes of high z/L_{rad} display the strongest scatter compared to the z/L dependence [Colour figure can be viewed at wileyonlinelibrary.com]

As both radiation divergence and sensible heat flux act on the temperature profile and vice versa, the interaction between radiation and convective processes defines the steady state of the atmosphere (Manabe and Strickler, 1964). Therefore, in what follows we further investigate the relationship between sensible heat flux, the atmospheric profiles and long-wave net flux divergence. We first try to understand how sensible heating and radiation can be related. We thus start with a theoretical analysis of radiative divergence in the surface layer. In the presence of radiative divergence, the conservation of potential temperature in a horizontally homogeneous surface layer reads:

$$\frac{\partial\overline{\theta}}{\partial t}=-\frac{\partial}{\partial z}\left(\overline{w'\theta'}+\frac{Rad}{\overline{\rho}C_p}\right), \tag{5}$$

with Rad the radiative flux. In a quasi-steady situation this implies that the divergence of the sum of sensible and radiative flux is constant in the surface layer (using a upward

positive convention for both turbulent and radiative fluxes). In the surface layer this variation with height is typically assumed to be small, i.e. we assume a constant flux layer, so that:

$$\overline{\rho} C_p \overline{w'\theta'} + Rad = \text{constant}. \quad (6)$$

The surface layer is also a region of near-constant momentum flux with height, so that we will further assume that u_* is constant. We can then define a locally varying temperature scaling, $\theta_*(z) = \overline{w'\theta'}(z)/u_*$, which varies with sensible heat flux vertical variations (and is defined as positive in stable conditions). Further neglecting radiative exchanges within the atmosphere, in a cloud-free atmosphere, we approximate the net long-wave radiation divergence, and thus the total radiative flux divergence, as the upward radiation divergence (as we neglect downward flux divergence, see next section). We thus focus only on upward long-wave radiation:

$$L_\uparrow \approx \varepsilon_s \pi B(T_s) - \overline{\varepsilon}(0 \to z)(\varepsilon_s \pi B(T_s) - \pi B(T)), \quad (7)$$

with B the long-wave blackbody radiation, $\overline{\varepsilon}$ the mean atmospheric emissivity, T_s the surface temperature and ε_s the surface emissivity. Combining Equations (6) and (7), evaluated at level z and at the surface $z=0$ and assuming that the surface emissivity is close to 1 so that reflected atmospheric radiation can be neglected:

$$\begin{aligned} &\overline{\rho} C_p u_* \theta_*(z) + \pi B(T_s) - \overline{\varepsilon}(0 \to z)(\pi B(T_s) - \pi B(T)) \\ &\quad = \overline{\rho} C_p u_* \theta_*(0) + \pi B(T_s). \end{aligned} \quad (8)$$

We can decompose the difference in radiation, neglecting the impact of surface emissivity (i.e. assumingε_s is close to 1), as: $B(T_s) - B(T) = [B(T_s) - B(T(z=0))] + [B(T(z=0)) - B(T)]$ so that the difference between T_s and T is apparent. Further linearizing the blackbody emission we obtain:

$$\begin{aligned} B(T_s) - B(T) = &\frac{dB}{dT}_{|\,T(z=0)} \underbrace{(T_s - T(z=0))}_{\equiv \Delta T} \\ &+ \frac{dB}{dT}_{|\,T} (T(z=0) - T). \end{aligned} \quad (9)$$

The right-hand side of Equation (9) can be related to the integral of the similarity function (if one still assumes validity of MOST): $T(z=0) - T = \frac{\theta_*(0)}{K}\left(\ln\left(\frac{z}{z_0}\right) - \Psi_h(z/L) + \Psi_h(z_0/L)\right)$ with Ψ_h the integral of the heat similarity function. We can first rewrite Equation (9):

$$\begin{aligned} B(T_s) - B(T) = &\frac{dB}{dT}_{|\,T(z=0)} \Delta T + \frac{dB}{dT}_{|\,T} \frac{\theta_*(0)}{K} \\ &\times \left(\ln\left(\frac{z}{z_0}\right) - \Psi_h(z/L) + \Psi_h(z_0/L)\right), \end{aligned} \quad (10)$$

and then finally rewrite Equation (10) as:

$$\begin{aligned} \overline{\rho} C_p u_* \theta_*(z) = &\overline{\rho} C_p u_* \theta_*(0) \left(1 + \frac{\overline{\varepsilon}(0 \to z)\pi}{\overline{\rho} C_p u_*} \frac{dB}{dT}_{|\,T} \right. \\ &\times \left. \left(\frac{1}{K}\left(\ln\left(\frac{z}{z_0}\right) - \Psi_h(z/L) + \Psi_h(z_0/L)\right)\right)\right) \\ &+ \frac{dB}{dT}_{|\,T(z=0)} \Delta T. \end{aligned} \quad (11)$$

Equation (11) emphasizes how the vertical variations in sensible heating are related to blackbody emission but also to the profile itself. It also highlights the importance of the difference between the surface skin temperature and air temperature, ΔT. At our site, which is humid and almost never reaches very hot temperatures, sensible heating remains small and so does ΔT but this term could be large in dry and hot semi-arid or arid regions as well as in polar regions. If we thus further neglect ΔT, at our site, we then get

$$\overline{\rho} C_p u_* \theta_*(z) = \overline{\rho} C_p u_* \theta_*(0) \left(1 + \frac{1}{\overline{\rho} C_p u_*} \underbrace{\overline{\varepsilon}(0 \to z)\pi \frac{dB}{dT}_{|\,T} \left(\frac{1}{K}\left(\ln\left(\frac{z}{z_{0,h}}\right) - \Psi_h(z/L) + \Psi_h(z_{0,h}/L)\right)\right)}_{\Delta L_\uparrow}\right), \quad (12)$$

which emphasizes the tight relationship between radiation divergence and sensible heating. This can be rewritten using the derivative of the blackbody emission: $\pi \frac{dB}{dT}_{|\,T} = 4\sigma T^3$.

In a near-neutral case, assuming a roughness length for momentum $z_{0,m}$ of 0.01 m and heat $z_{0,h}$ of 0.001 m for grass of height 0.1 m, and for a 1 m/s wind speed, gives sensible heat flux vertical variations due to radiative divergence of the order of 130% between 0.1 and 3.4 m (the height at which we were performing turbulent flux observations). Stable stratifications generate negative integral similarity function Ψ_h so that the relative effect of radiation divergence will be increased compared to the neutral case. We thus further evaluate the dependence between radiation divergence and sensible heating in the next section.

4.2 | Relationship between radiation divergence and surface sensible heat flux

To understand the coupling between radiation and turbulence, we investigate the relationship between long-wave radiation divergence and sensible heat flux. There is a strong (negative) correlation between long-wave net radiation flux divergence and surface sensible heat flux in non-foggy conditions (defined as relative humidity below 90%), as seen in Figure 10. This could be expected as sensible heat flux is directly coupled to the surface-layer temperature profile, which in turn acts back on the long-wave radiation divergence

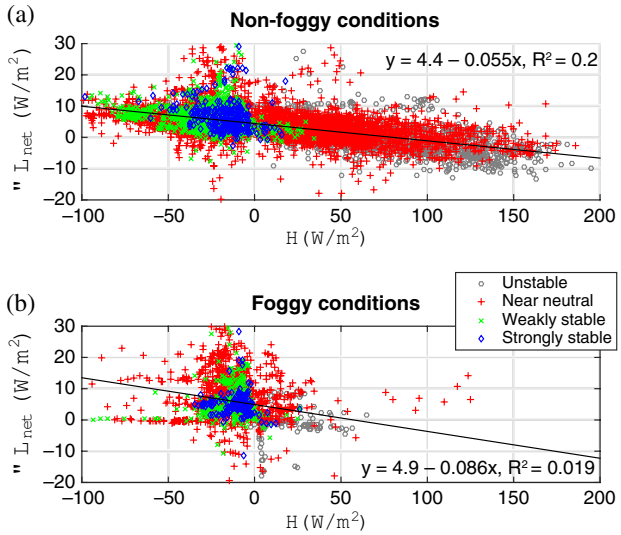

FIGURE 10 Dependence of long-wave radiative cooling ΔL_{net} on sensible heat flux in (a) non-foggy, and (b) foggy conditions defined as relative humidity above 90%. Buoyancy effects of water vapour lead to non-zero cut-off between stable and unstable conditions in terms of sensible heat flux [Colour figure can be viewed at wileyonlinelibrary.com]

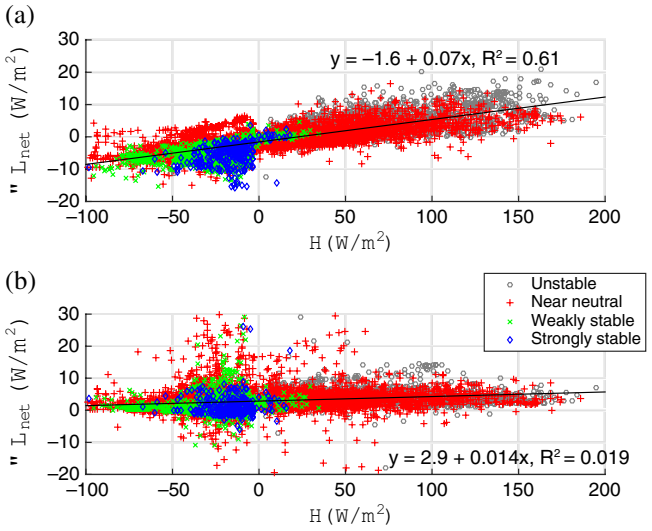

FIGURE 11 Long-wave (a) upward and (b) downward divergence, as a function of surface sensible heat flux in non-foggy conditions, defined as relative humidity less than 90%. Buoyancy effects of water vapour lead to non-zero cut-off between stable and unstable conditions in terms of sensible heat flux [Colour figure can be viewed at wileyonlinelibrary.com]

and indirectly on the humidity profile through the surface energy budget partitioning and related changes in Bowen ratio and latent heat flux, with the latter impacting the specific humidity profile. In turn, radiation directly impacts the stability of the profile (Manabe and Strickler, 1964), so it also modifies the surface turbulent fluxes though changes in stability.

In foggy conditions, the relationship between sensible heat flux and long-wave divergence weakens (Figure 10, bottom). As the long-wave divergence depends on the cloud thickness, relative humidity level and aerosols among other factors, the sensible heat flux is not the main influence on the temperature (and humidity) profile and therefore on the net long-wave divergence.

To further comprehend the relationship between radiation divergence and surface sensible heat flux, we decompose the net radiation into the upward and downward components (Figure 11). The upward radiation relates to the surface conditions whereas downward radiation reflects mostly the atmospheric state. As expected, the upward long-wave divergence $\Delta L_{\downarrow}$ correlates with sensible heat flux across stability conditions ($R^2 = 0.2$), even if some departure is observed in strongly stable conditions ($z/L > 0.5$). This decorrelation in stable conditions is not surprising as small or intermittent turbulence does not act as efficiently on the temperature profile, leading to near decorrelation between long-wave divergence and turbulence (Van de Wiel *et al.,* 2002a; 2002b; Holtslag *et al.,* 2007). Because of this decorrelation in the strongly stable boundary layer and since radiation divergence is an important term in the boundary-layer heat budget, this calls for accurate representation of long-wave divergence in very stable boundary layers, which is nonetheless typically overlooked compared to turbulent fluxes.

To further reduce the observed spread we normalize the upward and downward radiative flux by the absolute 1.3 m long-wave fluxes. In other words, we normalize the radiative divergence by the absolute radiation value, as the latter reflects diverse weather conditions as well as changes in surface emissivity and infrared temperature. Normalizing indeed reduces the spread for both the upward and downward divergence fluxes (Figure 12), especially for the downward radiation, which is strongly influenced by diverse weather conditions. The linear relationships (provided in Figure 13) could represent a simple alternative to representing radiative divergence in surface models without explicitly resolving an expensive high-vertical-resolution radiative transfer.

Holtslag and De Bruin (1988) showed that a relevant parameter to represent the coupled land-surface and stable boundary layer is θ_*/u_*. We thus further test this parameter in lieu of the sensible heat flux (Figure 13). Indeed using θ_*/u_* improves the upward divergence relationship, especially in the strongly stable boundary layer, where θ_*/u_* is the relevant scaling. The dependence of $\Delta L_{\downarrow}/L_{\downarrow}$ on θ_*/u_* is relatively tight across values, being nearly linear below $\theta_*/u_* \approx 1$ and then plateauing. Nonetheless, using θ_*/u_* does not improve the relative downward flux divergence $\Delta L_{\downarrow}/L_{\downarrow}$ and actually worsens the correlation compared to sensible heat flux.

Overall these results emphasize that in non-foggy conditions sensible heat flux and long-wave divergence are not independent variables but are coupled so that an extended MOST, including radiation divergence Equation 4, could be reduced to a simpler form similar to the regular MOST3, in which the dimensional temperature vertical gradient would be determined by the stability z/L only. In this case the radiation divergence term would be implicit yet we could expect some dependence based on the different

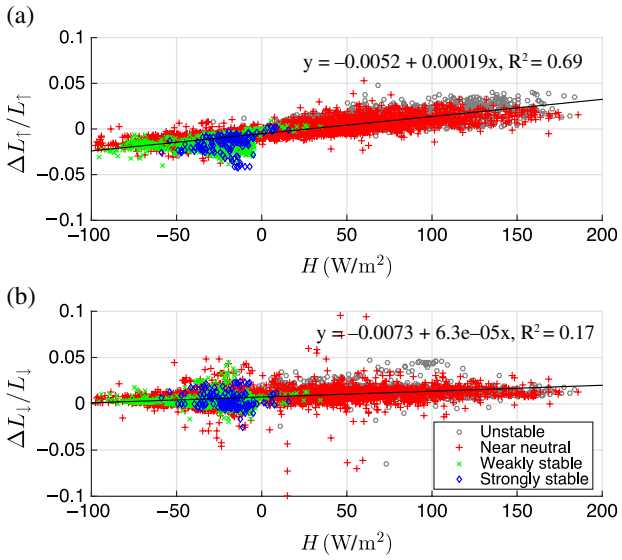

FIGURE 12 Normalized (a) upward and (b) downward long-wave divergence flux as a function of sensible heat flux H in non-foggy conditions, binned by stability conditions: Unstable ($z/L < -0.1$), near neutral ($|z/L| < 0.1$), weakly stable ($0.5 > z/L > 0.1$) and strongly stable ($z/L > 0.5$). Buoyancy effects of water vapour lead to non-zero cut-off between stable and unstable conditions in terms of sensible heat flux [Colour figure can be viewed at wileyonlinelibrary.com]

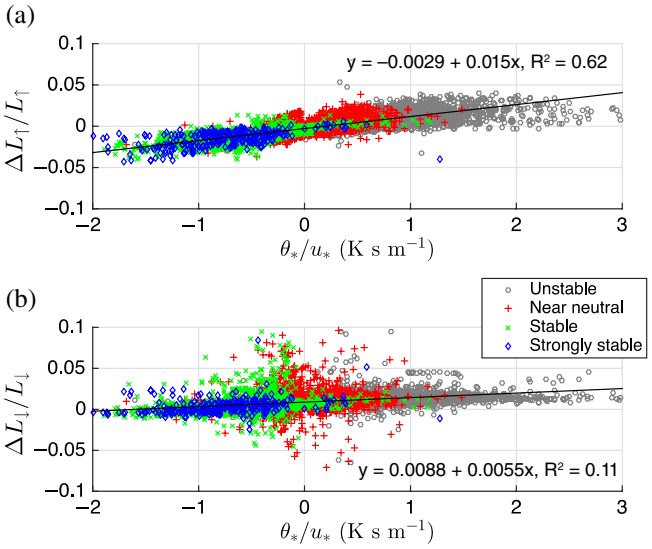

FIGURE 13 Normalized (a) upward and (b) downward long-wave divergence as a function of θ_*/u^* in non-foggy conditions (defined as relative humidity less than 90%). Buoyancy effects of water vapour lead to non-zero cut-off between stable and unstable conditions in terms of sensible heat flux. Upward and downward radiation fluxes are taken as positive in their respective direction. The divergence is computed as the difference between the value at 1.3 m minus the value at 20 m [Colour figure can be viewed at wileyonlinelibrary.com]

local conditions (atmospheric mean temperature and humidity, surface emissivity). In foggy situations, both long-wave divergence and sensible heat flux are needed to correctly describe the temperature profile as they are decoupled. In this case, the equation 4 still pertains because the radiative length-scales become independent from the Obukhov length. We thus suggest that future studies should perform independent *in situ* high-vertical-resolution measurements of radiative divergence fluxes and temperature gradient, along with surface turbulent flux measurements. High-resolution simulations and theoretical derivations will also help further disentangle radiation effects on surface layer turbulence.

5 | DISCUSSION

First, in land-surface models the air is assumed transparent in the long wave between the surface and the level (typically between 2 and 20 m) connected to the atmosphere (atmospheric model or weather station forcing in off-line models), so that there is no long-wave divergence. We have shown that long-wave net divergence flux acts as a strong cooling/heating term and is strongly coupled to surface sensible heat flux. In addition, even if atmospheric models should resolve the radiative flux divergence, they do not seem to reproduce the observed values and strongly underestimate the magnitude of the divergence, even when using high vertical resolution in the boundary layer (~20 m) (Steeneveld *et al.,* 2010). Possible reasons for this discrepancy includes: (a) too coarse vertical resolution to correctly capture the vertical gradients of temperature and trace gases, (b) incorrect model representation of those gradients, or (c) because the temporal resolution of the radiation scheme might not be sufficient to correctly represent the large-amplitude diurnal cycle of long-wave radiation. Indeed the radiation scheme is typically called in atmospheric models every 1–3 h because it is computationally expensive, generating a lag-induced warm bias at night (Vilà-Guerau de Arellano and Casso-Torralba, 2007). This could generate a systematic bias in coupled land–atmosphere models, as observed over continents (Clouds Above the United States and Errors at the Surface (CAUSES: Cheruy *et al.,* 2014; Van Weverberg *et al.,* 2015), especially if the connecting height between the land-surface model and the atmosphere is high, i.e. 10 m or so above the surface, as we have shown that divergence below 10 m was strong.

We encourage future field observations to resolve this issue. Also, the strong correlation in non-foggy conditions between surface sensible heat flux, long-wave divergence and temperature gradient emphasizes that to correctly derive surface layer similarity relationships, we need independent measurements of radiation divergence, surface turbulent flux and temperature gradient. Such data are unfortunately not available at present and might have polluted flux-gradient relationships; indeed, current relationships might implicitly represent some of the long-wave radiation divergence depending on the measurement heights used during the observation. This is an important issue that requires further attention.

6 | CONCLUSIONS

We have investigated the coupling of radiation divergence with turbulence in the atmospheric surface layer using

long-term observations at the Wageningen observatory, the Netherlands. The net radiation divergence appears to be a substantial term in the near-surface layer, not only at night but throughout the course of the day. The long-wave divergence term is the dominant term of the radiation divergence in the surface layer and is mostly present in the lower 10 m of the surface layer. Daily-mean values of temperature tendencies induced by long-wave radiation divergence of −10 to −20 K/day are typical.

Spectral analysis shows that it is challenging to identify the effect of long-wave radiation on the turbulent potential energy (TPE) dissipation and that it overall appears to have negligible impact on the temperature spectrum, at least in the conditions observed near Wageningen. Further high-resolution data acquisition of long-wave radiation at multiple levels would certainly help better constrain the magnitude of the radiation dissipation term.

We showed that sensible heat flux and long-wave divergence are strongly coupled, through changes in the surface layer profiles. Long-wave upward and downward divergence fluxes normalized by the absolute flux are correlated with sensible heat flux, so that a simple linear regression of $\Delta L_{\uparrow}/L_{\uparrow}$ and $\Delta L_{\downarrow}/L_{\downarrow}$ with surface sensible heat flux provides reasonable estimate of the directional components of the net divergence flux and its coupling to sensible heating. The advantage of the normalization by the magnitude of the flux is that it allows deriving a parametrization that is neither dependent on surface conditions (encapsulated in $L_{\downarrow}$) nor atmospheric conditions (encapsulated in $L_{\downarrow}$). This parametrization is sufficiently simple to be implemented in land-surface or weather/climate models, which typically assume that the air is transparent in the long-wave spectrum.

The present study raises several questions that could unfortunately not be answered with the present dataset. First, we may wonder whether previously derived flux-gradient relationships (e.g. Businger *et al.,* 1971; Beljaars and Holtslag, 1991) already implicitly accounted for radiation divergence; indeed, those observations used observed temperature profile gradients in the surface layer, which certainly included the effect of radiation. Nonetheless, radiation divergence was not measured independently of the surface heat fluxes so that the derived relationship might include it implicitly (Garratt and Brost, 1981). The implicit inclusion of radiation could be an additional explanation of the different similarity relationship between temperature and other scalars, especially under strongly stratified regimes, in addition to different turbulent effects in active and passive scalars (Li and Bou-Zeid, 2011).

A question is whether Monin–Obukhov Similarity Theory (MOST) should be modified to include radiative effects. A major issue is that different heights have been used to derive the temperature gradients depending on the observational campaign and in general are located within the region impacted by strong long-wave divergence. Measurements above the region of large radiation divergence should have been added to understand the behaviour of the profile in the absence of radiation (Garratt and Brost, 1981). This calls for multiple height measurements of both radiation and temperature along with surface turbulent fluxes to independently estimate the contributions of sensible and radiation flux to the temperature profile. This also emphasizes that an additional layer, the radiative layer in which radiative divergence is large, should be included when considering similarity theories.

In a landmark paper, Manabe and Strickler (1964) emphasized that both radiation and turbulent fluxes acted in concert and interactively to explain the temperature lapse rate of the atmosphere. Such a perspective on the surface and boundary layer has been somewhat limited to a few modelling and observational studies and should be evaluated more widely and in more detail through systematic observations. Such an understanding of the differential role of radiation and surface fluxes would be especially key in tropical and polar regions for accurate prediction of changes of the turbulent and radiation fluxes and their implications on changes in the surface temperature under global warming.

ACKNOWLEDGEMENTS

We thank three reviewers for their valuable feedbacks and comments on the manuscript. P. Gentine would like to thank Alan K. Betts for inspiring discussions on the role of radiation in the boundary layer. P. Gentine acknowledges funding from Grant NASA NIP 13-0095, DOE-FA-00085, NSF CAREER EAR 1552304 and DOE Early Career DE-SC0014203. The contribution by G.J. Steeneveld has been sponsored by the NWO contract 863.10.010 (Lifting the fog). Data used in this study can be made available on request to Bert Heusinkveld at bert.heusinkveld@wur.nl. They are stored on a local hard drive. Thirty-minute averaged datasets are available as Excel files. Turbulent data are available as text files.

ORCID

Pierre Gentine https://orcid.org/0000-0002-0845-8345
Gert-Jan Steeneveld https://orcid.org/0000-0002-5922-8179

REFERENCES

Albrecht, B.A. (1991) Fractional cloudiness and cloud-top entrainment instability. *Journal of the Atmospheric Sciences*, 48(12), 1519–1525.

Andre, J., Demoor, G., Lacarrere, P., Therry, G. and Duvachat, R. (1978) Modeling 24-hour evolution of mean and turbulent structures of planetary boundary-layer. *Journal of the Atmospheric Sciences*, 35(10), 1861–1883.

Baldocchi, D., Falge, E., Gu, L., Olson, R., Hollinger, D., Running, S., Anthoni, P., Bernhofer, C., Davis, K., Evans, R., Fuentes, J., Goldstein, A., Katul, G., Law, B., Lee, X., Malhi, Y., Meyers, T., Munger, W., Oechel, W., Paw, K.T., Pilegaard, K., Schmid, H.P., Valentini, R., Verma, S., Vesala, T., Wilson, K. and Wofsy, S. (2001) FLUXNET: a new tool to study the temporal

and spatial variability of ecosystem-scale carbon dioxide, water vapor, and energy flux densities. *Bulletin of the American Meteorological Society*, 82(11), 2415–2434.

Bechtold, P., Krueger, S.K., Lewellen, W.S., Van Meijgaard, E., Moeng, C.H., Randall, D.A., Van Ulden, A. and Wang, S. (1996) Modeling a stratocumulus-topped PBL: intercomparison among different one-dimensional codes and with large eddy simulation. *Bulletin of the American Meteorological Society*, 77(9), 2033–2042.

Beljaars, A.C.M. and Holtslag, A.A.M. (1991) Flux parameterization over land surfaces for atmospheric models. *Journal of Applied Meteorology*, 30, 327–341. https://doi.org/10.1175/1520-0450(1991)030<0327:FPOLSF>2.0.CO;2.

Betts, A.K., Desjardins, R. and Worth, D. (2013) Cloud radiative forcing of the diurnal cycle climate of the Canadian Prairies. *Journal of Geophysical Research Atmospheres*, 118(16), 8935–8953. https://doi.org/10.1002/jgrd.50593.

Blay-Carreras, E., Pardyjak, E.R., Pino, D., Alexander, D.C., Lohou, F. and Lothon, M. (2014) Countergradient heat flux observations during the evening transition period. *Atmospheric Chemistry and Physics*, 14(17), 9077–9085. https://doi.org/10.5194/acp-14-9077-2014.

Bony, S., Colman, R., Kattsov, V.M., Allan, R.P., Bretherton, C.S., Dufresne, J.L., Hall, A., Hallegatte, S., Holland, M.M., Ingram, W., Randall, D.A., Soden, B.J., Tselioudis, G. and Webb, M.J. (2006) How well do we understand and evaluate climate change feedback processes? *Journal of Climate*, 19(15), 3445–3482.

Brutsaert, W. (1972) Radiation, evaporation and the maintenance of turbulence under stable conditions in the lower atmosphere. *Boundary-Layer Meteorology*, 2, 309–325.

Burns, S.P., Sun, J., Delany, A.C., Semmer, S.R., Oncley, S.P. and Horst, T.W. (2003) A field intercomparison technique to improve the relative accuracy of longwave radiation measurements and an evaluation of CASES-99 pyrgeometer data quality. *Journal of Atmospheric and Oceanic Technology*, 20, 348–361.

Businger, J., Wyngaard, J., Izumi, Y. and Bradley, E. (1971) Flux-profile relationships in the atmospheric surface layer. *Journal of the Atmospheric Sciences*, 28(2), 181–189.

Cerni, T. and Parish, T. (1984) A radiative model of the stable nocturnal boundary layer with application to the polar night. *Journal of Applied Meteorology*, 23, 1563–1572.

Cheruy, F., Dufresne, J.L., Hourdin, F. and Ducharne, A. (2014) Role of clouds and land-atmosphere coupling in mid-latitude continental summer warm biases and climate change amplification in CMIP5 simulations. *Geophysical Research Letters*, 41, 6493–6500. https://doi.org/10.1002/2014GL061145.

Coantic, M. and Simonin, O. (1984) Radiative effects on turbulent temperature spectra and budgets in the planetary boundary layer. *Journal of the Atmospheric Sciences*, 41(17), 2629–2651. https://doi.org/10.1175/1520-0469(1984)041<2629:REOTTS>2.0.CO;2.

Deardorff, J.W. (1970) A numerical study of three-dimensional turbulent channel flow at large Reynolds numbers. *Journal of Fluid Mechanics*, 41(2), 453–480.

Deardorff, J.W. (1979) Prediction of convective mixed-layer entrainment for realistic capping inversion structure. *Journal of the Atmospheric Sciences*, 36(3), 424–436.

Deardorff, J.W. (1981) On the distribution of mean radiative cooling at the top of a stratocumulus-capped mixed layer. *Quarterly Journal of the Royal Meteorological Society*, 107(451), 191–202.

Dias, N.L. (2013) Reconciling radiation dissipation in the spatial and spectral domains under stable conditions. *Water Resources Research*, 49(10), 7150–7153. https://doi.org/10.1002/wrcr.20460.

Dias, N. and Brutsaert, W. (1998) Radiative effects on temperature in the stable surface layer. *Boundary-Layer Meteorology*, 89(1), 141–159.

Drüe, C. and Heinemann, G. (2007) Characteristics of intermittent turbulence in the upper stable boundary layer over Greenland. *Boundary-Layer Meteorology*, 124(3), 261–381. https://doi.org/10.1007/s10546-007-9175-8.

Edwards, J.M., Basu, S., Bosveld, F.C. and Holtslag, A.A.M. (2014) The impact of radiation on the GABLS3 large-eddy simulation through the night and during the morning transition. *Boundary-Layer Meteorology*, 152(2), 189–211. https://doi.org/10.1007/s10546-013-9895-x.

Estournel, C., Vehil, R. and Guedalia, D. (1986) An observational study of radiative and turbulent cooling in the nocturnal boundary layer (ECLATS experiment). *Boundary-Layer Meteorology*, 34, 55–62.

Fang, M., Albrecht, B.A., Ghate, V.P. and Kollias, P. (2013a) Turbulence in continental stratocumulus. Part I: External forcings and turbulence structures. *Boundary-Layer Meteorology*, 150, 341–360. https://doi.org/10.1007/s10546-013-9873-3.

Fang, M., Albrecht, B.A., Ghate, V.P. and Kollias, P. (2013b) Turbulence in continental stratocumulus. Part II: Eddy dissipation rates and large-eddy coherent structures. *Boundary-Layer Meteorology*, 150, 361–380. https://doi.org/10.1007/s10546-013-9872-4.

Fedorovich, E. (1995) Modeling the atmospheric convective boundary layer within a zero-order jump approach: an extended theoretical framework. *Journal of Applied Meteorology*, 34, 1916–1928.

Fedorovich, E., Conzemius, R. and Mironov, D. (2004) Convective entrainment into a shear-free, linearly stratified atmosphere: bulk models re-evaluated through large eddy simulations. *Journal of the Atmospheric Sciences*, 61(3), 281–295.

Fisher, J.B., Baldocchi, D.D., Misson, L., Dawson, T.E. and Goldstein, A.H. (2007) What the towers don't see at night: nocturnal sap flow in trees and shrubs at two AmeriFlux sites in California. *Tree Physiology*, 27, 597–610.

Garratt, J.R. and Brost, R.A. (1981) Radiative cooling effects within and above the nocturnal boundary layer. *Journal of the Atmospheric Sciences*, 38(12), 2730–2746. https://doi.org/10.1175/1520-0469(1981)038<2730:RCEWAA>2.0.CO;2.

Genthon, C., Six, D., Gallée, H. and Grigioni, P. (2013) Two years of atmospheric boundary layer observations on a 45-m tower at Dome C on the Antarctic plateau. *Journal of Geophysical Research: Atmospheres*, 118, 3218–3232. https://doi.org/10.1002/jgrd.50128.

Gentine, P. and Bellon, G. (2014) A closer look at boundary layer inversion in large-eddy simulations and bulk models: buoyancy-driven case. *Journal of the Atmospheric Sciences*, 72(2), 728–749. https://doi.org/10.1175/JAS-D-13-0377.1.

Gentine, P., Polcher, J. and Entekhabi, D. (2011) Harmonic propagation of variability in surface energy balance within a coupled soil-vegetation-atmosphere system. *Water Resources Research*, 47, 1–21. https://doi.org/10.1029/2010WR009268.

Gentine, P., Entekhabi, D. and Heusinkveld, B. (2012) Systematic errors in ground heat flux estimation and their correction. *Water Resources Research*, 48(9), W09541). https://doi.org/10.1029/2010WR010203.

Gentine, P., Betts, A.K. and Lintner, B.R. (2013) A probabilistic bulk model of coupled mixed layer and convection. Part I: Clear-sky case. *Journal of the Atmospheric Sciences*, 70(6), 1543–1556. https://doi.org/10.1175/JAS-D-12-0145.1.

Gu, L. and Baldocchi, D. (2002) Fluxnet 2000 synthesis: foreword. *Agricultural and Forest Meteorology*, 113, 1–2.

Ha, K.J. and Mahrt, L. (2003) Radiative and turbulent fluxes in the nocturnal boundary layer. *Tellus A*, 55(4), 317–327.

Heusinkveld, B., Jacobs, A., Holtslag, A. and Berkowicz, S. (2004) Surface energy balance closure in an arid region: role of soil heat flux. *Agricultural and Forest Meteorology*, 122(1–2), 21–37. https://doi.org/10.1016/j.agrformet.2003.09.005.

Hoch, S.W., Calanca, P., Philipona, R. and Ohmura, A. (2007) Year-round observation of longwave radiative flux divergence in Greenland. *Journal of Applied Meteorology and Climatology*, 46(9), 1469–1479. https://doi.org/10.1175/JAM2542.1.

Högström, U. (1996) Review of some basic characteristics of the atmospheric surface layer. *Boundary-Layer Meteorology*, 78, 215–246.

Holtslag, A.A.M. (2014) Introduction to the third GEWEX atmospheric boundary layer study (GABLS3). *Boundary-Layer Meteorology*, 152(2), 127–132. https://doi.org/10.1007/s10546-014-9931-5.

Holtslag, A.A.M. and De Bruin, H.A.R. (1988) Applied modeling of the nighttime surface energy balance over land. *Journal of Applied Meteorology*, 27, 689–704.

Holtslag, A.A.M. and Nieuwstadt, F.T.M. (1986) Scaling the atmospheric boundary layer. *Boundary-Layer Meteorology*, 36(1–2), 201–209. https://doi.org/10.1007/BF00117468.

Holtslag, A.A.M., Steeneveld, G.J. and van de Wiel, B.J.H. (2007) Role of land-surface temperature feedback on model performance for the stable boundary layer. In: *Atmospheric Boundary Layers*. New York, NY: Springer, pp. 205–220.

Huang, J. and Bou-Zeid, E. (2013) Turbulence and vertical fluxes in the stable atmospheric boundary layer. Part I: A large-eddy simulation study. *Journal of*

the Atmospheric Sciences, 70(6), 1513–1527. https://doi.org/10.1175/JAS-D-12-0167.1.

Jacobs, A.F.G., Heusinkveld, B.G., Wichink Kruit, R.J. and Berkowicz, S.M. (2006) Contribution of dew to the water budget of a grassland area in the Netherlands. *Water Resources Research*, 42(3), W03415. https://doi.org/10.1029/2005WR004055.

Kaimal, J.C., Wyngaard, J. and Haugen, D.A. (1976) Turbulence structure in the convective boundary layer. *Journal of the Atmospheric Sciences*, 33, 2152–2166.

Khanna, S. and Brasseur, J.G. (1997) Analysis of Monin–Obukhov similarity from large-eddy simulation. *Journal of Fluid Mechanics*, 345, 251–286.

Kleczek, M.A., Steeneveld, G.-J. and Holtslag, A.A.M. (2014) Evaluation of the weather research and forecasting mesoscale model for GABLS3: impact of boundary-layer schemes, boundary conditions and spin-up. *Boundary-Layer Meteorology*, 152(2), 213–243. https://doi.org/10.1007/s10546-014-9925-3.

Kolmogorov, A.N. (1941) The local structure of turbulence in incompressible viscous fluid for very large Reynolds numbers. *Proceedings: Mathematical and Physical Sciences*, 434, 9–13.

Kolmogorov, A.N. (1961) A refinement of previous hypotheses concerning the local structure of turbulence in a viscous incompressible fluid at high Reynolds number. *Journal of Fluid Mechanics*, 13(1), 82–85.

Lawrence, D.M., Oleson, K.W., Flanner, M.G., Thornton, P.E., Swenson, S.C., Lawrence, P.J., Zeng, X., Yang, Z.-L. and Levis, S. (2011) Parameterization improvements and functional and structural advances in Version 4 of the Community Land Model. *Journal of Advances in Modeling Earth Systems*, 3(1), 1–27. https://doi.org/10.1029/2011MS00045.

Li, D. and Bou-Zeid, E. (2011) Coherent structures and the dissimilarity of turbulent transport of momentum and scalars in the unstable atmospheric surface layer. *Boundary-Layer Meteorology*, 140(2), 243–262. https://doi.org/10.1007/s10546-011-9613-5.

Lothon, M., Lohou, F., Pino, D., Couvreux, F., Pardyjak, E.R., Reuder, J., Vilà-Guerau de Arellano, J., Durand, P., Hartogensis, O., Legain, D., Augustin, P., Gioli, B., Lenschow, D.H., Faloona, I., Yagüe, C., Alexander, D.C., Angevine, W.M., Bargain, E., Barrié, J., Bazile, E., Bezombes, Y., Blay-Carreras, E., van de Boer, A., Boichard, J.L., Bourdon, A., Butet, A., Campistron, B., de Coster, O., Cuxart, J., Dabas, A., Darbieu, C., Deboudt, K., Delbarre, H., Derrien, S., Flament, P., Fourmentin, M., Garai, A., Gibert, F., Graf, A., Groebner, J., Guichard, F., Jiménez, M.A., Jonassen, M., van den Kroonenberg, A., Magliulo, V., Martin, S., Martinez, D., Mastrorillo, L., Moene, A.F., Molinos, F., Moulin, E., Pietersen, H.P., Piguet, B., Pique, E., Román-Cascón, C., Rufin-Soler, C., Saïd, F., Sastre-Marugán, M., Seity, Y., Steeneveld, G.J., Toscano, P., Traullé, O., Tzanos, D., Wacker, S., Wildmann, N. and Zaldei, A. (2014) The BLLAST field experiment: boundary-layer late afternoon and sunset turbulence. *Atmospheric Chemistry and Physics*, 14(20), 10931–10960. https://doi.org/10.5194/acp-14-10931-2014.

Mahrt, L. (1999) Stratified atmospheric boundary layers. *Boundary-Layer Meteorology, 90(3), 375–396*.

Mamadou, O., de la Motte, L.G., De Ligne, A., Heinesch, B. and Aubinet, M. (2016) Sensitivity of the annual net ecosystem exchange to the cospectral model used for high frequency loss corrections at a grazed grassland site. *Agricultural and Forest Meteorology*, 228–229, 360–369. https://doi.org/10.1016/j.agrformet.2016.06.008.

Manabe, S. and Strickler, R.F. (1964) Thermal equilibrium of the atmosphere with a convective adjustment. *Journal of the Atmospheric Sciences*, 21, 361–385. https://doi.org/10.1175/1520-0469(1964)021<0361:TEOTAW>2.0.CO;2.

Mason, P.J. (1989) Large-eddy simulation of the convective atmospheric boundary layer. *Journal of the Atmospheric Sciences*, 46(11), 1492–1516.

Mauritsen, T., Svensson, G., Zilitinkevich, S.S., Esau, I., Enger, L. and Grisogono, B. (2007) A total turbulent energy closure model for neutrally and stably stratified atmospheric boundary layers. *Journal of the Atmospheric Sciences*, 64(11), 4113–4126. https://doi.org/10.1175/2007JAS2294.1.

Moeng, C., Sullivan, P. and Stevens, B. (1999) Including radiative effects in an entrainment rate formula for buoyancy-driven PBLs. *Journal of the Atmospheric Sciences*, 56(8), 1031–1049.

Naumann, A.K., Stevens, B., Hohenegger, C. and Mellado, J.P. (2017) A conceptual model of a shallow circulation induced by prescribed low-level radiative cooling. *Journal of the Atmospheric Sciences*, 74(10), 3129–3144. https://doi.org/10.1175/JAS-D-17-0030.1.

Nieuwstadt, F. and Businger, J.A. (1984) Radiative cooling near the top of a cloudy mixed layer. *Quarterly Journal of the Royal Meteorological Society*, 110, 1073–1078.

Pithan, F. and Mauritsen, T. (2014) Arctic amplification dominated by temperature feedbacks in contemporary climate models. *Nature Geoscience*, 7(3), 181–184. https://doi.org/10.1038/ngeo2071.

Randall, D.A. (1980) Entrainment into a stratocumulus layer with distributed radiative cooling. *Journal of the Atmospheric Sciences*, 37(1), 148–159.

Rauber, R.M., Stevens, B., Ochs, H.T., III, Knight, C., Albrecht, B.A., Blyth, A.M., Fairall, C.W., Jensen, J.B., Lasher-Trapp, S.G., Mayol-Bracero, O.L., Vali, G., Anderson, J.R., Baker, B.A., Bandy, A.R., Burnet, E., Brenguier, J.L., Brewer, W.A., Brown, P.R.A., Chuang, R., Cotton, W.R., di Girolamo, L., Geerts, B., Gerber, H., Göke, S., Gomes, L., Heikes, B.G., Hudson, J.G., Kollias, P., Lawson, R.R., Krueger, S.K., Lenschow, D.H., Nuijens, L., O'Sullivan, D.W., Rilling, R.A., Rogers, D.C., Siebesma, A.P., Snodgrass, E., Stith, J.L., Thornton, D.C., Tucker, S., Twohy, C.H. and Zuidema, P. (2007) Rain in shallow cumulus over the ocean – the RICO campaign. *Bulletin of the American Meteorological Society*, 88(12), 1912–1928. https://doi.org/10.1175/BAMS-88-12-1912.

Schertzer, D. and Simonin, O. (1982) A theoretical study of radiative cooling in homogeneous and isotropic turbulence. In: *Turbulent Shear Flows 3*. Berlin, Heidelberg: Springer, pp. 262–274.

Schmidt, H. and Schumann, U. (2006) Coherent structure of the convective boundary layer derived from large-eddy simulations. *Journal of Fluid Mechanics*, 200, 511–562. https://doi.org/10.1017/S0022112089000753.

Sorbjan, Z. (1991) Evaluation of local similarity functions in the convective boundary-layer. *Journal of Applied Meteorology*, 30(12), 1565–1583.

Steeneveld, G.J., Wokke, M., Zwaaftink, C. and Pijlman, S. (2010) Observations of the radiation divergence in the surface layer and its implication for its parameterization in numerical weather prediction models. *Journal of Geophysical Research*, 115(D6), D06107. https://doi.org/10.1029/2009JD013074.

Sterk, H., Steeneveld, G.J., A, A. and Holtslag, M. (2013) The role of snow-surface coupling, radiation, and turbulent mixing in modeling a stable boundary layer over Arctic sea ice. *Journal of Geophysical Research: Atmospheres*, 118, 1199–1217.

Stevens, B. and Moeng, C.H. (1999) Large-eddy simulations of radiatively driven convection: sensitivities to the representation of small scales. *Journal of the Atmospheric Sciences*, 56(23), 3963–3984.

Stevens, B., Ackerman, A.S., Albrecht, B.A., Brown, A.R., Chlond, A., Cuxart, J., Duynkerke, P.G., Lewellen, D.C., Macvean, M.K., Neggers, R.A.J., Sánchez, E., Siebesma, A.P. and Stevens, D.E. (2001) Simulations of trade wind cumuli under a strong inversion. *Journal of the Atmospheric Sciences*, 58(14), 1870–1891.

Stull, R.B. (1988) *An Introduction to Boundary Layer Meteorology*. (Vol. 13). Springer Science & Business Media.

Sullivan, P., Moeng, C., Stevens, B., Lenschow, D. and Mayor, S. (1998) Structure of the entrainment zone capping the convective atmospheric boundary layer. *Journal of the Atmospheric Sciences*, 55(19), 3042–3064.

Tennekes, H. (1973) A model for the dynamics of the inversion above a convective boundary layer. *Journal of the Atmospheric Sciences*, 30(4), 558–567.

Tennekes, H. and Driedonks, A. (1981) Basic entrainment equations for the atmospheric boundary layer. *Boundary-Layer Meteorology*, 20, 515–531.

Townsend, A.A. (1958) The effects of radiative transfer on turbulent flow of a stratified fluid. *Journal of Fluid Mechanics*, 4(4), 361–375. https://doi.org/10.1017/S0022112058000501.

Van de Wiel, B., Moene, A., Ronda, R., De Bruin, H. and Holtslag, A.A.M. (2002a) Intermittent turbulence and oscillations in the stable boundary layer over land. Part II: A system dynamics approach. *Journal of the Atmospheric Sciences*, 59(17), 2567–2581.

Van de Wiel, B., Ronda, R., Moene, A., De Bruin, H. and Holtslag, A.A.M. (2002b) Intermittent turbulence and oscillations in the stable boundary layer over land. Part I: A bulk model. *Journal of the Atmospheric Sciences*, 59(5), 942–958. https://doi.org/10.1175/1520-0469(2002)059<0942:ITAOIT>2.0.CO;2.

Van Weverberg, K., Morcrette, C.J., Ma, H.-Y., Klein, S.A. and Petch, J.C. (2015) Using regime analysis to identify the contribution of clouds to surface temperature errors in weather and climate models. *Quarterly Journal of the Royal Meteorological Society*, 141(693), 3190–3206. https://doi.org/10.1002/qj.2603.

Vilà-Guerau de Arellano, J. and Casso-Torralba, P. (2007) The radiation and energy budget in mesoscale models: an observational study case. *Fisica de la Terra*, 17, 117–132.

Wang, Q. and Albrecht, B. (2000) Observations of cloud-top entrainment in marine stratocumulus clouds. *Journal of the Atmospheric Sciences*, 51, 1–18.

Webb, E.K., Pearman, G.I. and Leuning, R. (1980) Correction of flux measurements for density effects due to heat and water vapour transfer. *Quarterly Journal of the Royal Meteorological Society*, 106(447), 85–100. https://doi.org/10.1002/qj.49710644707.

Wilson, K., Goldstein, A., Falge, E., Aubinet, M., Baldocchi, D., Berbigier, P., Bernhofer, C., Ceulemans, R., Dolman, H., Field, C., Grelle, A., Ibrom, A., Law, B.E., Kowalski, A., Meyers, T., Moncrieff, J., Monson, R., Oechel, W., Tenhunen, J., Valentini, R. and Verma, S. (2002) Energy balance closure at FLUXNET sites. *Agricultural and Forest Meteorology*, 113(1–4), 223–243. https://doi.org/10.1016/S0168-1923(02)00109-0.

SUPPORTING INFORMATION

Additional supporting information may be found online in the Supporting Information section at the end of the article.

How to cite this article: Gentine P, Steeneveld G-J, Heusinkveld BG, Holtslag AA. Coupling between radiative flux divergence and turbulence near the surface. *Q J R Meteorol Soc* 2018;144:2491–2507. https://doi.org/10.1002/qj.3333